44th AIAA Aerospace Sciences Meeting and Exhibit
9 - 12 January 2006, Reno, Nevada

AIAA 2006-49

A Continuous Adjoint Method for the Minimization of Losses in Cascade Viscous Flows

Dimitrios I. Papadimitriou* and Kyriakos C. Giannakoglou†

Lab. of Thermal Turbomachines,

National Technical University of Athens,

P.O. Box 64069, 15710 Athens, GREECE

A continuous adjoint formulation for the minimization of viscous losses in laminar cascade flows is presented. The losses are expressed in terms of entropy generation due to the boundary layer formation and development. The minimization of the entropy difference between the inlet to and outlet from the flow domain results from the minimization of a field integral, expressed in terms of the velocity gradient. For the latter, appropriate field adjoint equations along with boundary conditions are derived, leading to sensitivity derivatives depending only upon wall boundary terms. The Lagrange multiplier penalty method is used to handle geometrical constraints related to the minimum allowed thickness of the designed cascade airfoils. For the sake of comparison, a discrete adjoint method was also programmed and used for the solution of the same problem, in which the total pressure losses, instead of the entropy increase, was used as the objective function.

I. Introduction

In Computational Fluid Dynamics, the formulation and numerical solution of the so–called adjoint equations is the means of computing the objective function gradient required by deterministic optimization methods. In the literature, continuous and discrete adjoint methods have been devised and proposed. In the former, the adjoint equations are derived from the flow equations by considering them as constraints to the objective function and are, then, discretized accordingly.[1–4] In the discrete adjoint method, the discrete adjoint equations are derived from the discretized flow equations.[5,6] Through either variant, the objective function gradient is computed with the same CPU cost regardless of the number of design variables; this cost is by far less than that of finite–difference schemes. The adjoint approach was introduced by Pironneau[7] for elliptic problems and extended to transonic flows by Jameson.[8,9]

The treatment of the objective function reflects a major difference between continuous and discrete methods. In the discrete method, the objective function merely acts as a right–hand–side term in the adjoint equations. Regardless of where the objective function has been defined, viz. either over the whole domain or just along its boundary, the treatment is the same. Any objective function is admissible which is not the case in continuous adjoint. Current research on continuous adjoint methods focuses on the formulation of the adjoint equations and boundary conditions for objective functions which are theoretically inadmissible, though of engineering interest.[10]

In this paper, an objective function which quantifies losses in viscous layer dominated flows is employed and, based on it, both continuous and discrete adjoint methods are formulated and tested. The optimization of a compressor airfoil cascade is used to demonstrate convincingly that the proposed method works well. However, the formulation is general and may become useful in many other internal aerodynamics design problem, such as the design of optimal ducts. The mimimum loss requirement is expressed as the minimization of the entropy increase from the inlet to the outlet of the domain. The proposed formulation takes into account only the part of entropy generated within the viscous layers and the objective functional takes the form of a field integral with integrand depending mainly on the velocity gradient. In the past, the

*PhD Student, National Technical University of Athens, dpapadim@mail.ntua.gr
†Associate Professor, National Technical University of Athens, kgianna@central.ntua.gr

theoretical backround of the proposed objective function was used to compute viscous losses associated with $2D$ turbomachinery flows[11–13] and, in the present work, is used in design–optimization problems. According to the development shown below, the resulting sensitivity derivatives are cast in the form of boundary integrals along solid walls. Note that this is not really necessary in the development of the discrete adjoint method, in which the objective function is just the difference between total pressure integrals over the inlet and outlet boundaries, but is extremely useful for the continuous adjoint. Finally, in both methods, extra Lagrange multipliers are introduced to account for geometrical constraints: the design of the cascade airfoil is subjected to constraints related to minimum allowed thicknesses at several longitudinal positions.

II. Flow Equations and Objective Function

The Navier–Stokes equations for 2D laminar flows of perfect gases are written as

$$\frac{\partial \mathbf{U}}{\partial t} + \frac{\partial \mathbf{f}_i^{inv}}{\partial x_i} - \frac{\partial \mathbf{f}_i^{vis}}{\partial x_i} = \mathbf{0} \tag{1}$$

where

$$\mathbf{U} = h \begin{bmatrix} \rho \\ \rho \mathbf{V} \\ E \end{bmatrix} \ , \ \mathbf{f}_i^{inv} = h \begin{bmatrix} \rho u_i \\ \rho u_i \mathbf{V} + p\delta_i \\ u_i(E+p) \end{bmatrix} \ , \ \mathbf{f}_i^{vis} = h \begin{bmatrix} 0 \\ \tau_i \\ u_j \tau_{ij} + q_i \end{bmatrix} \tag{2}$$

and $\tau_i = [\tau_{i1}, \tau_{i2}]^T$ are the viscous stresses, with

$$\tau_{ij} = \mu(\frac{\partial u_i}{\partial x_j} + \frac{\partial u_j}{\partial x_i}) + \lambda \delta_{ij} \frac{\partial u_k}{\partial x_k} \quad , \quad \lambda = -\frac{2}{3}\mu \tag{3}$$

Also, $\delta_i = [\delta_{i1}, \delta_{i2}]^T$ are the Kronecker symbols, $\mathbf{V} = [u_1, u_2]^T$ is the velocity vector, $q_i = k\frac{\partial T}{\partial x_i}$ and $E = \rho e + \frac{1}{2}\rho u_i^2$. The Einstein convention applies for repeated indices.

The entropy s generation due to viscous effects over the flow domain Ω is determined by subtracting the mass averaged integral of s at the inlet S_i from the corresponding quantity at the outlet S_o, namely

$$F = \int_{S_o} s d\dot{m} - \int_{S_i} s d\dot{m} = \int_{S_{i,o}} \rho V_n s dS = \int_S \rho V_n s dS \tag{4}$$

It is evident that the contribution of solid walls and periodic boundaries to the integrals in Eq. (4) is zero, so the last expression is also true. Using the Gauss' divergence theorem and the continuity equation, Eq. (4) is transformed to a field integral over the flow domain Ω, as follows

$$F = \int_\Omega \rho u_i \frac{\partial s}{\partial x_i} d\Omega \tag{5}$$

or[11–13]

$$F = \int_\Omega \frac{1}{T} \tau_{ij} \frac{\partial u_i}{\partial x_j} d\Omega \tag{6}$$

The variation in the so–called augmented objective function δF_{aug} is derived by adding the inner product of the vector of costate variables $\mathbf{\Psi}$ and the variation in the flow equations to the variation in the objective function (i.e. Eq. (6)); so

$$\delta F_{aug} = \delta F + \int_\Omega \mathbf{\Psi}^T \delta(\frac{\partial \mathbf{f}_i^{inv}}{\partial x_i} - \frac{\partial \mathbf{f}_i^{vis}}{\partial x_i}) d\Omega \tag{7}$$

III. Formulation of the Adjoint Equations

Any further development of Eq. (7) is based on the following relationship.

$$\delta(\frac{\partial \Phi}{\partial x_i}) = \frac{\partial(\delta\Phi)}{\partial x_i} - \frac{\partial \Phi}{\partial x_k} \frac{\partial(\delta x_k)}{\partial x_i} \tag{8}$$

which can be proved after subtracting

$$\frac{\partial(\delta\Phi)}{\partial x_i} \;=\; \frac{\partial}{\partial x_i}(\frac{\partial\Phi}{\partial \mathbf{b}})\delta\mathbf{b} \;+\; \frac{\partial^2\Phi}{\partial x_i\partial x_k}\delta x_k \;+\; \frac{\partial\Phi}{\partial x_k}\frac{\partial(\delta x_k)}{\partial x_i} \tag{9}$$

from

$$\delta(\frac{\partial\Phi}{\partial x_i}) \;=\; \frac{\partial^2\Phi}{\partial x_i\partial x_k}\delta x_k \;+\; \frac{\partial}{\partial \mathbf{b}}(\frac{\partial\Phi}{\partial x_i})\delta\mathbf{b} \tag{10}$$

where $\mathbf{b}$ is the array of design variables. Eq. (9) expresses the derivative of the variation in Φ

$$\delta\Phi = \frac{\partial\Phi}{\partial \mathbf{b}}\delta\mathbf{b} \;+\; \frac{\partial\Phi}{\partial x_j}\delta x_j \tag{11}$$

with respect to x_i, while Eq. (10) expresses the variation in $\frac{\partial\Phi}{\partial x_i}$. Based on Eq. (8), the integral on the r.h.s. of Eq. (7) becomes

$$\int_\Omega \mathbf{\Psi}^T\delta\left(\frac{\partial\mathbf{f}_i}{\partial x_i}\right)d\Omega = \int_\Omega \mathbf{\Psi}^T\frac{\partial(\delta\mathbf{f}_i)}{\partial x_i}d\Omega - \int_\Omega \mathbf{\Psi}^T\frac{\partial\mathbf{f}_i}{\partial x_k}\frac{\partial(\delta x_k)}{\partial x_i}d\Omega \tag{12}$$

where $\mathbf{f}_i$ stands for either $\mathbf{f}_i^{inv}$ or $\mathbf{f}_i^{vis}$.

Development of the Inviscid Terms

By first considering the inviscid fluxes, both terms on the r.h.s. of Eq. (12) are integrated by parts and, after some mathematical rearrangements, we get

$$\begin{aligned}\int_\Omega \mathbf{\Psi}^T\delta\left(\frac{\partial\mathbf{f}_i^{inv}}{\partial x_i}\right)d\Omega \;=\; & -\int_\Omega\left(\delta\mathbf{U}^T - \frac{\partial\mathbf{U}}{\partial x_k}^T\delta x_k\right)\left(A_i^T\frac{\partial\mathbf{\Psi}}{\partial x_i}\right) + \int_\Omega \mathbf{\Psi}^T\frac{\partial}{\partial x_k}\left(\frac{\partial\mathbf{f}_i^{inv}}{\partial x_i}\right)\delta x_k d\Omega - \\ & \int_{S_w}\frac{\partial\mathbf{U}}{\partial x_k}^T {A_n}^T\mathbf{\Psi}\delta x_k dS + \int_{S_w}\Psi_{i+1}n_i\delta p dS + \\ & \int_{S_w}(\Psi_{i+1}p - \mathbf{\Psi}^T\mathbf{f}_i)\delta(n_i dS) + \int_{S_{i,o}}\delta\mathbf{U}^T(A_n^T\mathbf{\Psi})dS\end{aligned} \tag{13}$$

where A_i are the Jacobian matrices, $A_n = A_i n_i$ and n_i are the components of the outward normal vector at any boundary edge of the flow domain. Summation is implied for $i = 1, 2$.

Development of the Viscous Terms

Starting point for the development of the viscous terms in Eq. (12) is a relationship that is similar to Eq. (8) and governs variations in second–order derivatives. It could readily be shown that

$$\delta(\frac{\partial^2\Phi}{\partial x_i\partial x_j}) = \frac{\partial^2(\delta\Phi)}{\partial x_i\partial x_j} - \frac{\partial^2\Phi}{\partial x_i\partial x_k}\frac{\partial(\delta x_k)}{\partial x_j} - \frac{\partial^2\Phi}{\partial x_j\partial x_k}\frac{\partial(\delta x_k)}{\partial x_i} - \frac{\partial\Phi}{\partial x_k}\frac{\partial^2(\delta x_k)}{\partial x_j\partial x_i} \tag{14}$$

Through Eq. (14) and the identity $\tau_{ij}n_i n_j = 0$, the viscous term in Eq. (7) gives

$$\begin{aligned}&\int_\Omega \mathbf{\Psi}^T\delta\left(\frac{\partial\mathbf{f}_i^{vis}}{\partial x_i}\right)d\Omega = -\int_\Omega\left(\delta\mathbf{W} - \frac{\partial\mathbf{W}}{\partial x_k}\delta x_k\right)^T\mathbf{K}d\Omega - \int_\Omega \mathbf{\Psi}^T\frac{\partial}{\partial x_k}\left(\frac{\partial\mathbf{f}_i^{vis}}{\partial x_i}\right)\delta x_k d\Omega + \\ &\int_{S_w}\delta u_i\left[\mu\left(\frac{\partial\Psi_{j+1}}{\partial x_i} + u_j\frac{\partial\Psi_m}{\partial x_i} + \frac{\partial\Psi_{i+1}}{\partial x_j} + u_i\frac{\partial\Psi_m}{\partial x_j}\right) + \lambda\delta_{ij}\left(\frac{\partial\Psi_{k+1}}{\partial x_k} + u_k\frac{\partial\Psi_m}{\partial x_k}\right) - \Psi_4\tau_{ij}\right]n_j dS + \\ &\int_{S_w}\delta T\left(k\frac{\partial\Psi_4}{\partial x_i}n_i\right)dS - \int_{S_w}\Psi_4\delta(q_j n_j dS) + \int_{S_w}\Psi_4 q_j\delta(n_j dS) - \\ &\int_{S_w}\frac{\Psi_{i+1}}{n_i}[\delta\tau_{ij}n_i n_j + \tau_{ij}\delta(n_i n_j)]dS + \int_{S_w}\frac{\Psi_{i+1}}{n_i}\tau_{ij}\delta(n_i n_j)dS - \int_{S_w}u_i\Psi_4\delta\tau_{ij}n_j dS - \\ &\int_{S_w}\frac{\partial u_i}{\partial x_l}\left[\mu\left(\frac{\partial\Psi_{j+1}}{\partial x_i} + u_j\frac{\partial\Psi_m}{\partial x_i} + \frac{\partial\Psi_{i+1}}{\partial x_j} + u_i\frac{\partial\Psi_m}{\partial x_j}\right) + \lambda\delta_{ij}\left(\frac{\partial\Psi_{k+1}}{\partial x_k} + u_k\frac{\partial\Psi_m}{\partial x_k}\right)\right]\delta x_l n_j dS + \\ &\int_{S_w}\frac{\partial T}{\partial x_k}\left(k\frac{\partial\Psi_4}{\partial x_i}\right)\delta x_k n_i dS - \int_{S_w}\mathbf{\Psi}^T\frac{\partial\mathbf{f}_i^{vis}}{\partial x_k}\delta x_k n_i dS\end{aligned} \tag{15}$$

where

$$K_1 = -\frac{T}{\rho}\frac{\partial}{\partial x_i}\left(k\frac{\partial \Psi_4}{\partial x_i}\right)$$
$$K_{i+1} = \frac{\partial}{\partial x_j}\left[\mu\left(\frac{\partial \Psi_{j+1}}{\partial x_i}+u_j\frac{\partial \Psi_m}{\partial x_i}+\frac{\partial \Psi_{i+1}}{\partial x_j}+u_i\frac{\partial \Psi_m}{\partial x_j}\right)+\lambda\delta_{ij}\left(\frac{\partial \Psi_{k+1}}{\partial x_k}+u_k\frac{\partial \Psi_m}{\partial x_k}\right)\right]-\tau_{ij}\frac{\partial \Psi_4}{\partial x_j}$$
$$K_4 = \frac{T}{p}\frac{\partial}{\partial x_i}\left(k\frac{\partial \Psi_4}{\partial x_i}\right)$$

Here, $\mathbf{W} = [\rho, \mathbf{V}, p]^T$ is the vector of non–conservative variables and $i = 1, 2$.

Development of δF in Eq. (6)

The variation in the objective function F, as defined in Eq. (6), is analyzed below. The variation in gradients is first transformed to gradients of variation using Eq. (8) and, then, the Gauss' divergence theorem is employed. The term depending on the variation in the incremental volume $\delta(d\Omega)$ is written as

$$\delta(d\Omega) = \frac{\partial(\delta x_k)}{\partial x_k}d\Omega \tag{16}$$

By doing so, we have

$$\begin{aligned}\delta F = & -\int_\Omega \frac{\mu}{T^2}R\left(\delta T-\frac{\partial T}{\partial x_i}\delta x_i\right)d\Omega-\int_\Omega\frac{\partial}{\partial x_j}\left(\frac{\mu}{T}R_{ij}\right)\left(\delta u_i-\frac{\partial u_i}{\partial x_k}\delta x_k\right)d\Omega- \\ & \int_{S_w}\frac{\mu}{T}R_{ij}\frac{\partial u_j}{\partial x_k}n_i\delta x_k dS+\int_{S_w}\frac{\mu}{T}R\delta x_i n_i dS+\int_{S_w}\frac{\mu}{T}R_{ij}n_j\delta u_i dS\end{aligned} \tag{17}$$

where

$$R = \tau_{ij}\frac{\partial u_i}{\partial x_j} \quad , \quad R_{ij} = 2(1+\delta_{ij})\frac{\partial u_i}{\partial x_j}+2(1-\delta_{ij})\frac{\partial u_j}{\partial x_i}-\frac{4}{3}\delta_{ij}\frac{\partial u_k}{\partial x_k}$$

Adjoint Equations, Boundary Conditions and Sensitivity Derivatives

Eqs. (13), (15) and (17) determine the field adjoint equations, the inlet, outlet and wall boundary conditions for $\mathbf{\Psi}$ and, finally, the gradient of the objective function with respect to the design variables.[14] The system of the field adjoint equations is written as

$$\frac{\partial \mathbf{\Psi}}{\partial t}-A_i^T\frac{\partial \mathbf{\Psi}}{\partial x_i}-M^{-T}\mathbf{K}-M^{-T}\mathbf{L}=\mathbf{0} \tag{18}$$

where $M = \frac{\partial \mathbf{U}}{\partial \mathbf{W}}$ and $L = (L_1, L_2, L_3, L_4)^T$ with

$$\begin{aligned}L_1 &= \frac{1}{T^2}R\frac{\partial T}{\partial \rho}\\ L_{i+1} &= \frac{1}{T^2}R\frac{\partial T}{\partial u_i}\frac{\partial}{\partial x_j}\left(\frac{\mu}{T}R_{ij}\right)\\ L_4 &= \frac{1}{T^2}R\frac{\partial T}{\partial E}\end{aligned}$$

The boundary conditions of $\mathbf{\Psi}$ over the solid walls are selected so as to eliminate the terms $\int_{S_w}\Psi_{i+1}n_i\delta p dS$, $\int_{S_w}\frac{\Psi_{i+1}}{n_i}[\delta\tau_{ij}n_in_j+\tau_{ij}\delta(n_in_j)]dS$, $\int_{S_w}\delta T\left(k\frac{\partial\Psi_4}{\partial x_i}n_i\right)dS$ and $\int_{S_w}\Psi_4\delta(q_jn_jdS)$. For Ψ_2 and Ψ_3, zero Dirichlet conditions are imposed. For constant wall temperature, $\Psi_4 = 0$; otherwise, for adiabatic walls, $\frac{\partial\Psi_4}{\partial n} = 0$. The inlet, outlet conditions are defined so as to eliminate $\delta\mathbf{U}^T(A_n^T\mathbf{\Psi}) = 0$.

After defining the field and boundary adjoint equations, the remaining terms provide the objective function gradient

$$\delta F_{aug} = -\int_{S_w}\left(\mathbf{\Psi}^T\mathbf{f}_i\right)\delta(n_idS)-\int_{S_w}\frac{\partial \mathbf{U}^T}{\partial x_k}(A_i{}^Tn_i)\mathbf{\Psi}\delta x_k dS+$$

$$\int_{S_w}\left(\mathbf{\Psi}^T\frac{\partial \mathbf{f}_{vi}}{\partial x_k}\right)\delta x_k n_i dS+\int_{S_w}\Psi_4 q_j\delta(n_j dS)-$$
$$\int_{S_w}\frac{\partial u_i}{\partial x_l}\left[\mu\left(\frac{\partial\Psi_{j+1}}{\partial x_i}+u_j\frac{\partial\Psi_m}{\partial x_i}+\frac{\partial\Psi_{i+1}}{\partial x_j}+u_i\frac{\partial\Psi_m}{\partial x_j}\right)+\lambda\delta_{ij}\left(\frac{\partial\Psi_{k+1}}{\partial x_k}+u_k\frac{\partial\Psi_m}{\partial x_k}\right)\right]\delta x_l n_j dS-$$
$$\int_{S_w}R_{ij}\frac{\partial u_j}{\partial x_k}n_i\delta x_k dS+\int_{S_w}\frac{1}{T}R\delta x_i n_i dS \tag{19}$$

Eq. (19) clearly shows that, even though the objective function was defined as a field integral of losses, the sensitivity derivatives are expressed in terms of quantities computed only along the wall boundaries S_w.

IV. The Discrete Adjoint Approach

The discrete adjoint formulation is straightforward, without being affected by the definition of the objective function. So, there is no reason to use the field integral, Eq. (6), and the averaged total pressure loss between the inlet and outlet of Ω is used instead. The new objective function is

$$F \;=\; \frac{\int_{S_i}p_t dS}{S_i} \;-\; \frac{\int_{S_o}p_t dS}{S_o} \tag{20}$$

By multiplying the adjoint variable vector $\mathbf{\Psi}$ with the gradient of the discretized flow equations $\frac{d\mathbf{R}}{db}$ and adding it to the objective function gradient, the gradient of F_{aug} yields

$$\frac{dF_{aug}}{d\mathbf{b}} \;=\; \left(\frac{\partial F}{\partial \mathbf{U}}+\mathbf{\Psi}^T\frac{\partial \mathbf{R}}{\partial \mathbf{U}}\right)\frac{d\mathbf{U}}{d\mathbf{b}}+\frac{\partial F}{\partial \mathbf{b}}+\mathbf{\Psi}^T\frac{\partial \mathbf{R}}{\partial \mathbf{b}} \tag{21}$$

The discrete adjoint equation is

$$\left(\frac{\partial \mathbf{R}}{\partial \mathbf{U}}\right)^T\mathbf{\Psi}=-\left(\frac{\partial F}{\partial \mathbf{U}}\right)^T \tag{22}$$

and the remaining terms in Eq. (21) provide the objective function gradient with respect to the design variables, namely

$$\frac{dF_{aug}}{db} \;=\; \frac{\partial F}{\partial \mathbf{b}}+\mathbf{\Psi}^T\frac{\partial \mathbf{R}}{\partial \mathbf{b}} \tag{23}$$

Note that the first term on the r.h.s. of Eq. (23) is equal to zero because the objective function F is defined at the inlet and outlet of the domain and does not depend explicitly on the design variables. However, an implicit dependence is "hidden" in the second term and, of course, in the solution to the adjoint equations. The second term is computed using a central finite–difference scheme, in which the design variables are perturbed one by one, maintaining the same flow field and the residuals of the discrete flow equations R are computed.

V. The Constrained Optimization Method

Apart from the flow equations, which are treated as equality constraints with the adjoint variables $\mathbf{\Psi}$ as Lagrange multipliers, n geometrical inequality constraints should be satisfied too. These are related to the minimum allowed thickness of the optimal airfoil. Inequality constraints ($C_i \le 0$) are handled through the Lagrange multiplier theory together with penalty functions; the inequality constrained problem is converted to an equality constrained one by introducing additional variables.[15]

In the present cascade airfoil design, the thickness at certain positions along the airfoil chord, should be greater than user–defined values. The constrained minimization problem

$$\begin{aligned} &min \;\; F_{aug} \\ &s.t. \;\; C_i \le 0 \;\;,\;\; i=1,n \end{aligned} \tag{24}$$

is transformed to the following one

$$\begin{aligned} &min \;\; F_{aug} \\ &s.t. \;\; C_i+z_i^2=0 \;\;,\;\; i=1,n \end{aligned} \tag{25}$$

in which z_i are the additional variables to be optimized. The constraint–augmented objective function is

$$F_{c,aug} = F_{aug} + P_c \tag{26}$$

with

$$P_c = \sum_{i=1,n} \lambda_i (C_i + z_i^2) + \sum_{i=1,n} \frac{w}{2} (C_i + z_i^2)^2$$

where λ_i are the additional Lagrange multipliers and w is the penalty coefficient. The optimal value for z_i^2 is given by $z_i^2 = max[0, -(\frac{\lambda_i}{w} + C_i)]$ and the Lagrange multipliers are updated as follows: $\lambda_i^{k+1} = \lambda_i^k + w^k (C_i^k + z_i^2)$. Should any constraint be violated, its derivative with respect to the design variables is calculated analytically and added to the augmented function gradient. Otherwise, the steepest descent with variable step size is used: $\mathbf{b}^{k+1} = \mathbf{b}^k - \eta \frac{\delta F_{aug}}{\delta \mathbf{b}}$.

VI. Results–Discussion

The problem of the minimization of viscous losses in the flow developed through a two–dimensional compressor cascade, by redesigning its airfoil shape, is analyzed. The analysis tool is a time–marching Navier–Stokes equations solver for structured grids, based on the finite–volume technique and an upwind formulation, employing the Roe's approximate Riemann solver[16] with variables' extrapolation to account for second-order accuracy. Bezier polynomials are used to parameterize each blade side. Thirteen control points are used for each side. The optimization takes into consideration a number of geometrical constraints in order to avoid creating unacceptably thin airfoils. The objective function is either the entropy generation (continuous adjoint) or the total pressure losses (discrete adjoint).

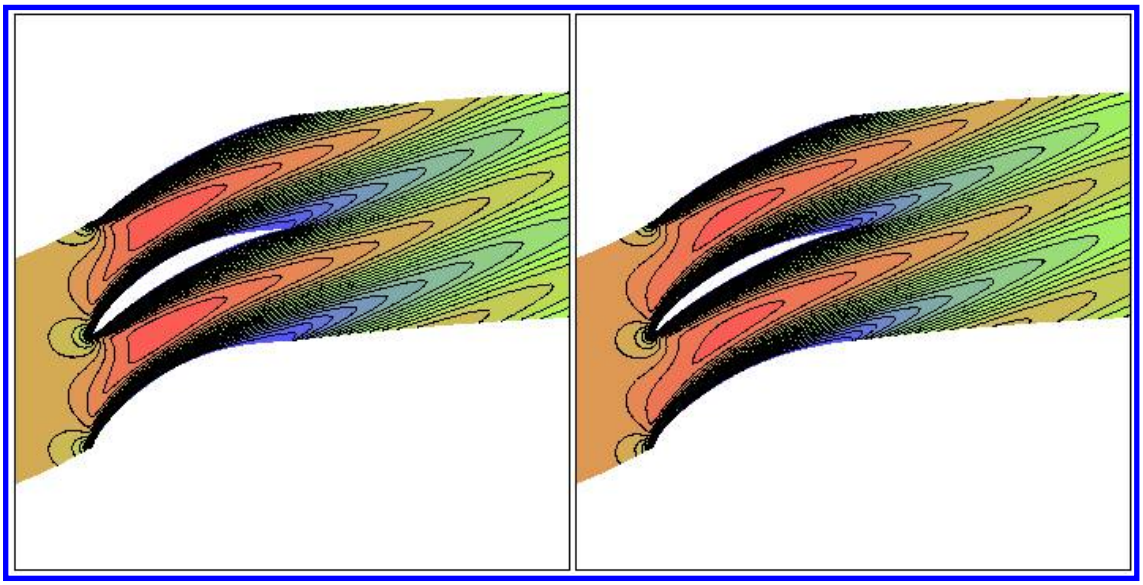

Figure 1. Mach number distribution over the initial (left) and optimal (right) airfoil cascade.

The flow is considered to be laminar with $\alpha_{in} = 50^o$, $M_{out,is} = 0.2$ and $Re_c = 1000$. In figure 1, the Mach number distributions over the initial and optimal (in particular, that computed using the continuous adjoint method) airfoil cascades are shown. Figure 2 shows the friction (left) and pressure (right) coefficient distributions over the initial (top) and optimal (continuous adjoint: middle; discrete adjoint: bottom) airfoils. The optimal airfoils, which are slightly different since they have been computed using different objective functions, present a milder deceleration of the flow over the rear part of the suction side. The initial and optimal airfoil contours, together with the location of the corresponding control points are shown in figure 3, for the continuous (left) and discrete (right) adjoint.

The next figures show the convergence rate of the constrained optimization algorithm for both approaches. Since different objective functionals are used (entropy generation and total pressure losses), both quantities

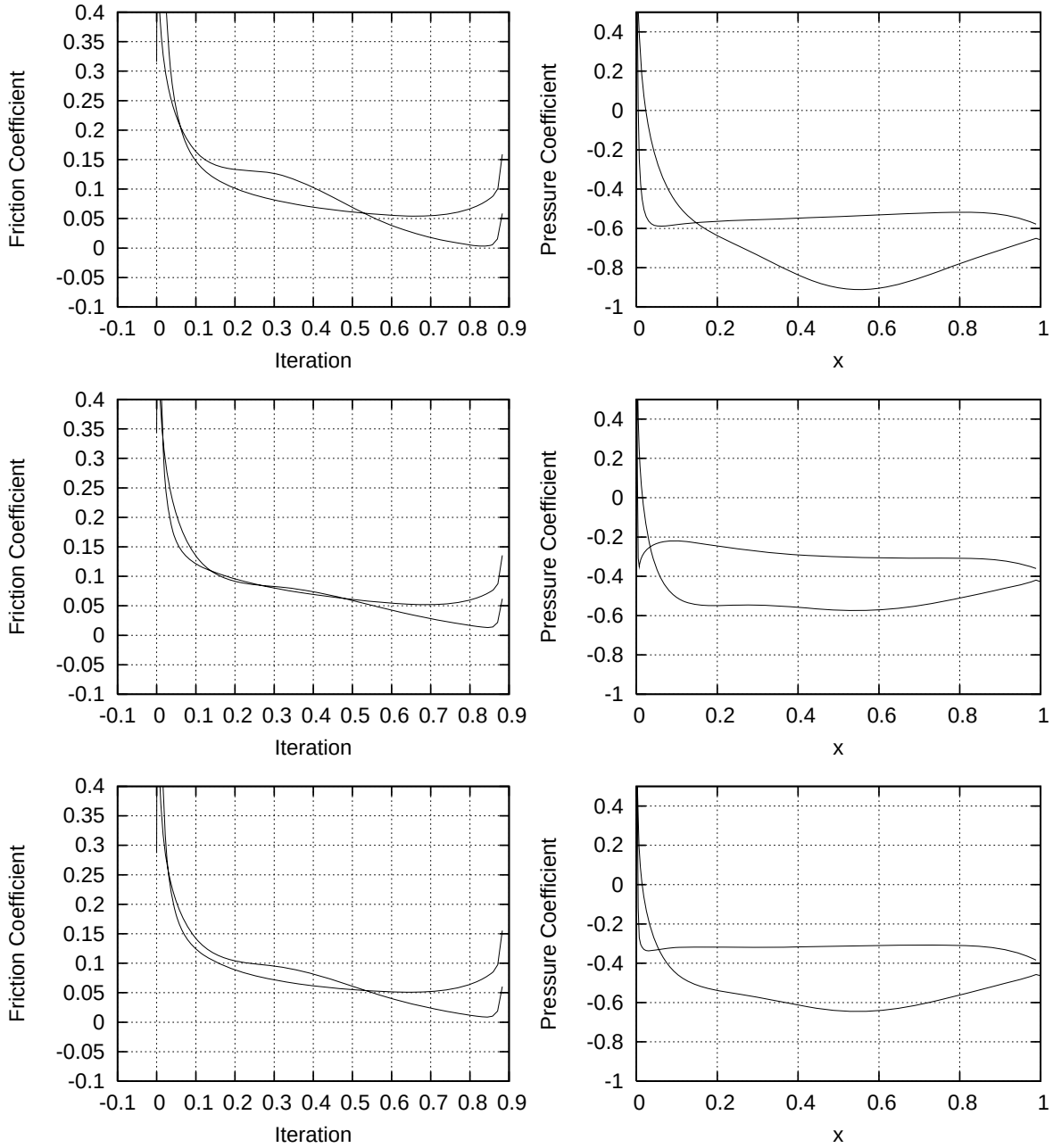

Figure 2. Left: Friction Coefficient, right: Pressure Coefficient for the initial (top), and optimal airfoil using the continuous (middle) and discrete (bottom) adjoint method.

have been plotted in order to compare the two algorithms, figure 4. Even though the objective functions used correspond only to the ordinates in the top–left and the bottom–right figures (i.e. the top–right and bottom–left figures are the results of postprocessing), all of the presented plots reveal the same tendency and, consequently, the equivalence of the two objective functions. Some spikes that appear during the first iterations are due to the handling of constraints which allowes us to come up with some infeasible (provisional, however) shapes.

Various quantities related to the geometrical constraints are also plotted. Figure 5, top, shows the evolution of the sum of thickness deviations $\sum_{i=1,n}(t_i - \tilde{t}_i)$ from the user–defined minimum thicknesses $\tilde{t}_i$. In both methods, the starting "thick" airfoil is identical, so $\sum_{i=1,n}(t_i - \tilde{t}_i) > 0$. Upon convergence, this quantity approaches zero. Since it is expressed as the algebraic sum of $(t_i - \tilde{t}_i)$, in the same figure (bottom)

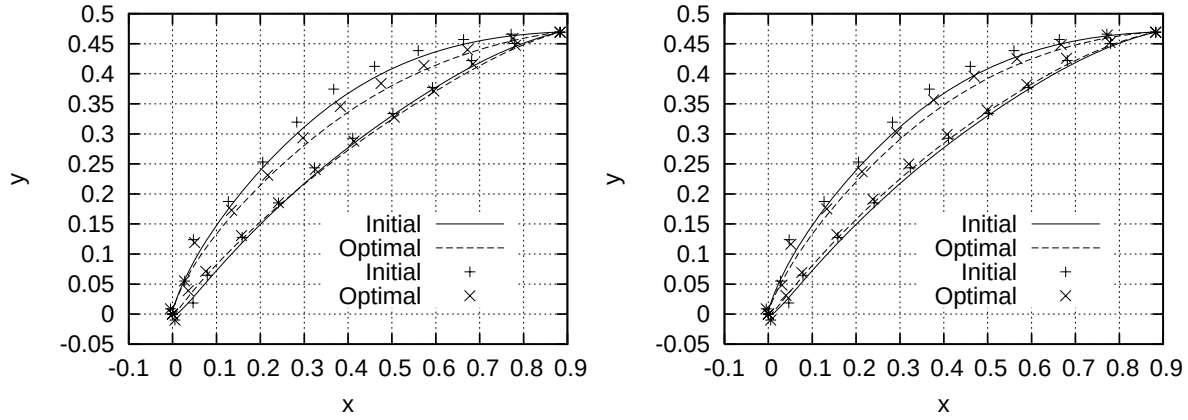

Figure 3. Initial and optimal blade contour and control points using the continuous (left) and discrete (right) adjoint method.

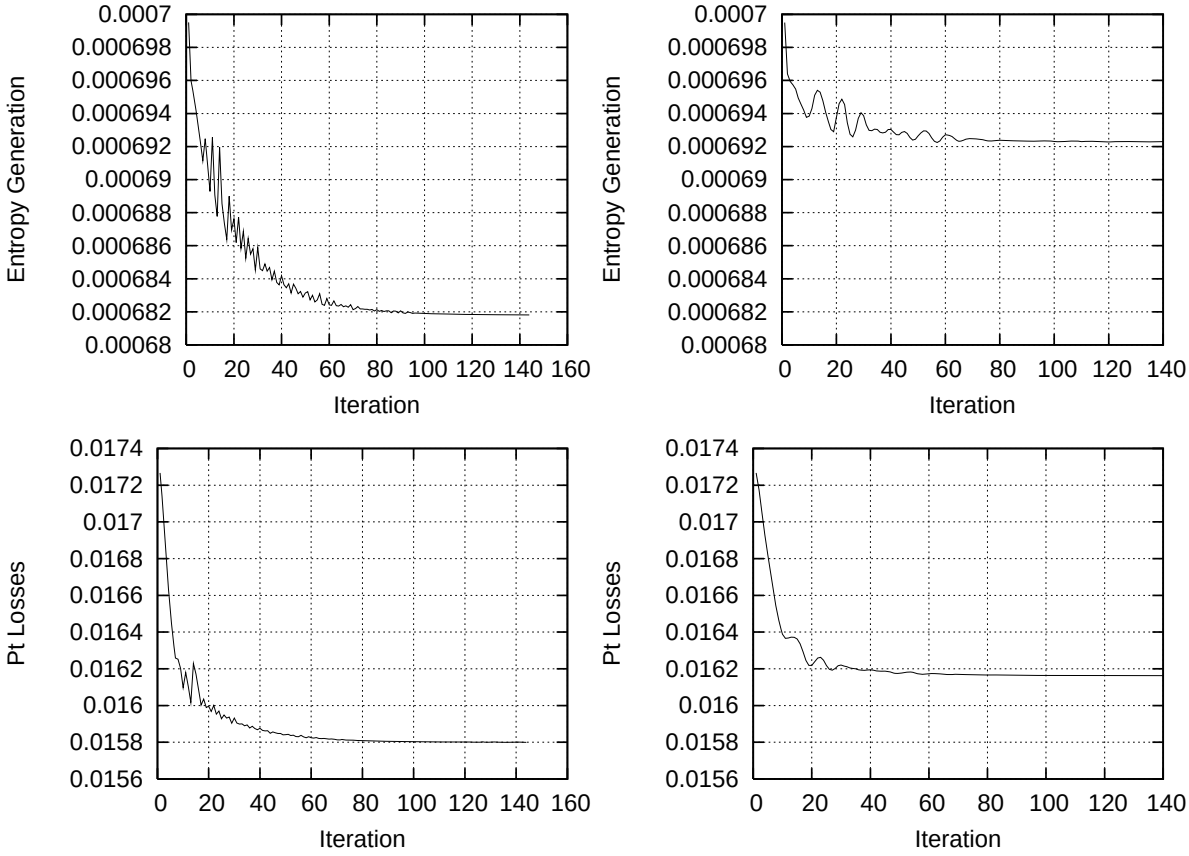

Figure 4. Convergence rate for the two objective functions, using the continuous (left) and discrete (right) adjoint method.

the quantity $\sum_{i=1,n} max(t_i - \tilde{t}_i, 0)$ is plotted. It now becomes clear that the computed optimal airfoils do not violate any of the constraints.

By further examining figure 5, we conclude that the airfoil designed through the discrete adjoint method is slightly thicker than that resulted from the continuous method. This explains why the continuous adjoint is able to yield comparatively lower losses, figure 4. From the numerical point of view, this difference can be attributed to the way the stepsize η as well as the penalty coefficient w vary during the steepest descent

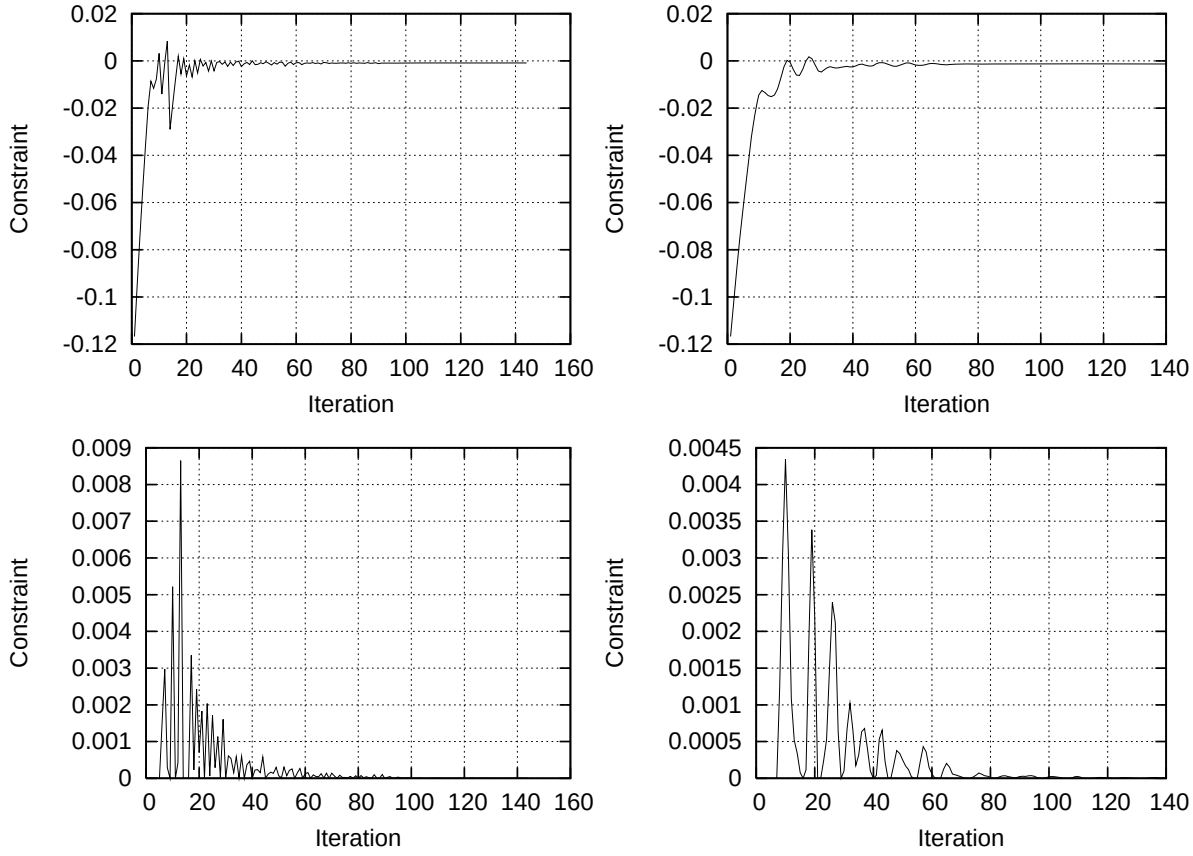

Figure 5. Convergence rate of $\sum_{i=1,n}(t_i - \tilde{t}_i)$ (top) and $\sum_{i=1,n} max(t_i - \tilde{t}_i, 0)$ (bottom) using the continuous (left) and discrete (right) adjoint method.

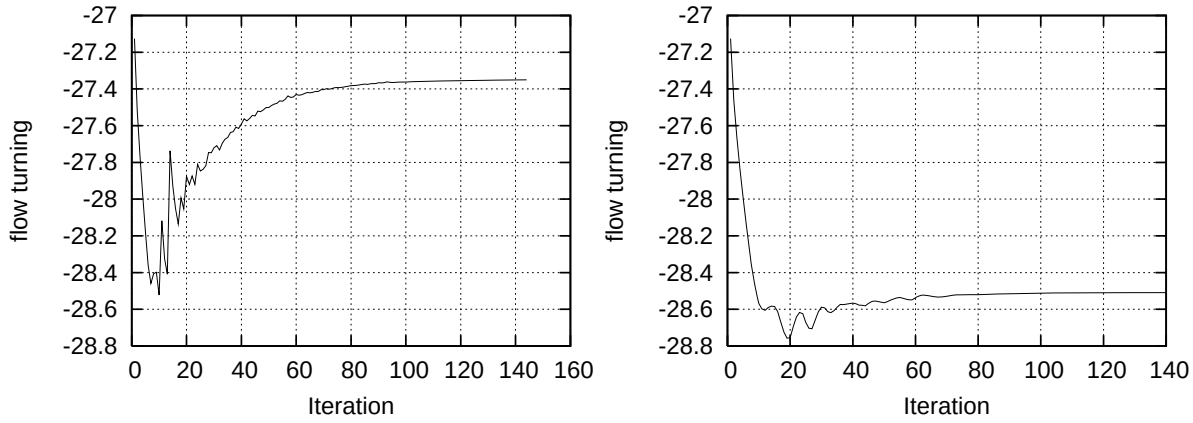

Figure 6. Monitoring of the convergence rate for the flow turning function using the continuous (left) and discrete (right) adjoint method.

algorithm.

It is also interesting to plot and comment on the convergence history of the flow turning through the cascade, figure 6. From this figure, it turns out that, during the first iterations, the flow turning increases, whereas losses reduce. However, as the optimization goes on, losses are reduced even more and new airfoil shapes are generated with less flow turning which finally stabilize at 27.4^o (continuous adjoint) or 28.5^o (discrete adjoint).

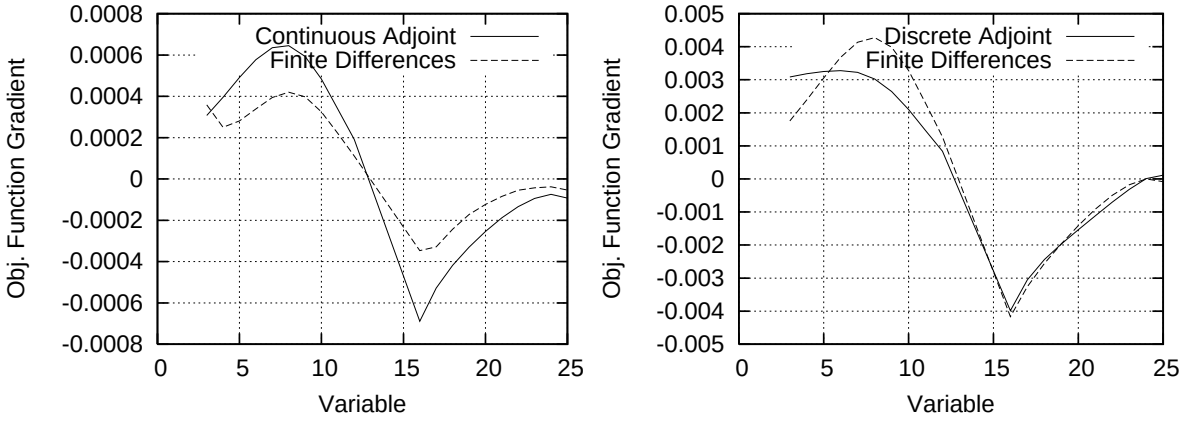

Figure 7. Objective function gradient computed through the continous (left) and the discrete (right) adjoint method and a central finite–difference scheme for the initial (the same in either method) airfoil.

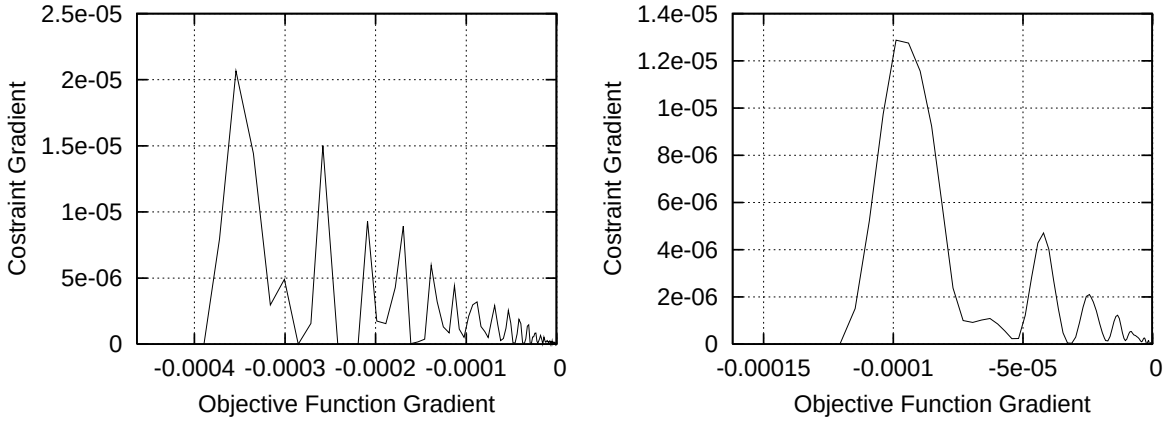

Figure 8. Objective function gradient norm, computed through the continous (left) and discrete (right) adjoint method against the constraint gradient norm.

Values of objective function gradient components are compared to those computed using a finite–difference scheme, figure 7. Both plots correspond to the same starting airfoil shape and the agreement between adjoint methods and finite–differences is satisfactory.

Figure 8 plots the convergence of the objective function gradient norm against the constraint gradient norm. In order to prevent the algorithm from terminating before reaching the (feasible) optimal solution the steepest descent stepsize was allowed to vary/decrease so that the constraint "takes its time" to converge as well.

VII. Conclusions

The problem of designing aerodynamic shapes with minimum viscous losses was addressed. An objective function based on the entropy generation in viscous layers, which is appropriate for use in continuous adjoint methods, was presented. It was demonstrated that the field integral defined in terms of the velocity gradient after the necessary rearrangement of terms, leads to admissible adjoint equations and boundary conditions along with sensitivity derivatives which depend only on integrals considered over the solid walls. In the examined test problem, i.e. the optimization of a compressor cascade airfoil, the comparison with a discrete adjoint method (using the averaged total pressure losses as objective), demonstrates the equivalence of the two formulations. Over and above, geometrical constraints related to the minimum airfoil thickness at various chordwise locations are imposed and handled using extra Lagrange multipliers and penalty functions.

Acknowledgments

The project is co–funded by the European Social Fund (75%) and National Resources (25%) - Operational Program for Educational and Vocational Training (EPEAEK) and particularly the Program IRAKLITOS.

References

[1]Jameson, A., Reuther, J., *Control Theory Based Airfoil Design using the Euler Equations*, AIAA Paper 94-4272-CP, 1994.

[2]Jameson, A., Alonso, J.J., Reuther, J.J., Martinelli, L., Vassberg, J.C., *Aerodynamic Shape Optimization Techniques Based on Control Theory*, AIAA Paper 98-2538, 1998.

[3]Jameson, A., Pierce, N., Martinelli, L., *Optimum Aerodynamic Design Using the Navier–Stokes Equations*, J. Theor. Comp. Fluid. Mech, 10, 213-237, 1998.

[4]Anderson, W.K., Venkatakrishnan, V., *Aerodynamic Design Optimization on Unstructured Grids with a Continuous Adjoint Formulation*, Computers and Fluids, 28, 443-480, 1999.

[5]Giles, M.B., *An Introduction to the Adjoint Approach to Design*, ERCOFTAC Workshop on Adjoint Methods, Toulouse, June 21-23, 1999.

[6]Giles, M.B., *Adjoint Methods for Aeronautical Design*, ECCOMAS CFD Conference, 2001.

[7]Pironneau, O., *Optimal Shape Design for Elliptic Systems*, Springer-Verlag, New-York, 1984.

[8]Jameson, A., *Aerodynamic Design via Control Theory*, Journal of Scientific Computation, 3, 33-260, 1988.

[9]Jameson, A., *Optimum Aerodynamic Design using CFD and Control Theory*, AIAA Paper 95-1729-CP, 1995.

[10]Arian, E., Salas, M.D., *Admitting the Inadmissible: Adjoint Formulation for Incomplete Cost Functionals in Aerodynamic Optimization*, NASA/CR-97-206269, ICASE Report No.97-69, 1997.

[11]Denton, J.D., *Loss Mechanisms in Turbomachines*, ASME Paper 93-GT-435, 1993.

[12]Davies, M.R.D., O'Donnell, F.K., Niven, A.J., *Turbine Blade Entropy Generation Rate, Part I: The Boundary Layer Defined*, ASME Paper 2000-GT-265, 2000.

[13]O'Donnell, F.K., Davies, M.R.D., *Turbine Blade Entropy Generation Rate, Part II: The Measured Loss*, ASME Paper 2000-GT-266, 2000.

[14]D.I. Papadimitriou, K.C.Giannakoglou, *A Continuous Adjoint Method with Objective Function Derivatives Based on Boundary Integrals for Inviscid and Viscous Flows*, Journal of Computers and Fluids, to appear, 2006.

[15]Bertsekas, D.P., *Constrained Optimization and Lagrange Multiplier Methods*, Athena Scientific, 1996.

[16]Roe, P., *Approximate Riemann Solvers, Parameter Vectors and Difference Schemes*, Journal of Computational Physics, 43, 357-371, 1981.

This article has been cited by:

1. Carlos Lozano. 2019. Entropy and Adjoint Methods. *Journal of Scientific Computing* **81**:3, 2447-2483. [Crossref]
2. Benjamin Walther, Siva Nadarajah. 2015. Adjoint-Based Constrained Aerodynamic Shape Optimization for Multistage Turbomachines. *Journal of Propulsion and Power* **31**:5, 1298-1319. [Abstract] [Full Text] [PDF] [PDF Plus]
3. Benjamin Walther, Siva Nadarajah. 2013. Constrained Adjoint-Based Aerodynamic Shape Optimization of a Single-Stage Transonic Compressor. *Journal of Turbomachinery* **135**:2. . [Crossref]
4. Benjamin Walther, Sivakumaran Nadarajah. Constrained Adjoint-Based Aerodynamic Shape Optimization in a Multistage Turbomachinery Environment . [Citation] [PDF] [PDF Plus]
5. Jiaqi Luo, Juntao Xiong, Feng Liu, Ivan McBean. 2011. Three-Dimensional Aerodynamic Design Optimization of a Turbine Blade by Using an Adjoint Method. *Journal of Turbomachinery* **133**:1. . [Crossref]
6. A.S. Zymaris, D.I. Papadimitriou, K.C. Giannakoglou, C. Othmer. 2009. Continuous adjoint approach to the Spalart–Allmaras turbulence model for incompressible flows. *Computers & Fluids* **38**:8, 1528-1538. [Crossref]
7. Dimitrios I. Papadimitriou, Kyriakos C. Giannakoglou. 2008. Aerodynamic Shape Optimization Using First and Second Order Adjoint and Direct Approaches. *Archives of Computational Methods in Engineering* **15**:4, 447-488. [Crossref]
8. D.I. Papadimitriou, K.C. Giannakoglou. 2008. Computation of the Hessian matrix in aerodynamic inverse design using continuous adjoint formulations. *Computers & Fluids* **37**:8, 1029-1039. [Crossref]